

Deep space laser communication transmitter and high precision timing system for small satellites

Paul Serra, Nathan Barnwell, Tyler Ritz, John W. Conklin
University of Florida

Mechanical and Aerospace Engineering, 231 MAE-A Building, P.O. Box 116250, Gainesville, FL 32611-6250; 1-352-392-9129
pserra@ufl.edu

ABSTRACT

The Miniature Optical Communication Transmitter is a NASA-sponsored compact, pulsed optical communication system for distant, power-constrained small satellites. A pulse-based scheme is driven by an FPGA-based Software-Defined Pulse Modulator. In addition to optical communication, the MOCT also has potential capabilities in precision clock synchronization and navigation beyond Earth orbit. This work is a continuation of results presented at the 2015 SmallSat conference.¹ A novel combinatorial delay generation technic allow a 10-fold increase in timing resolution and a similar improvement for delay uncertainties compared to previously reported results. The Laser system prototype is now complete and can operate with some amplification.

INTRODUCTION

Spacecraft communications using optical frequencies is widely recognized as a potentially more power efficient scheme compared to radio frequency communications. The higher wavelengths of optical systems drastically reduce the signal spread due to diffraction, and therefore reduce the amount of energy required to close the link. Pulsed optical communications systems allow to concentrate the energy further, by delivering most of the photons in a short period of time, with modest average power levels. The high peak power and short duration of the pulses enable their detection over long distance, where the quantity of received photons

The Precision Space Systems Laboratory (PSSL) at the University of Florida is developing a pulsed laser transmitter. The Miniature Optical Communications Transmitter (MOCT) is a compact pulsed laser transmitter with a target mass and power consumption level of 2 kg and < 10 W while transmitting. A prototype implementation of this technology is currently being developed to TRL 3 by 2017.

The MOCT is built upon two main subsystems: the Software Defined Pulse Modulator (SDPM) and the Master Oscillator Power Fiber Amplifier (MOPFA) laser system. The precision timing technologies and electronics are built upon components developed for the Optical Precision Time-transfer Instrument (OPTI). OPTI is a PSSL instrument which will demonstrate ground-to-space clock synchronization to 100 ps during a planned 2017 CubeSat flight.²

The MOPFA system is a 1550 nm fiber laser with target pulse widths of 100 ps and pulse energies of ~ 1 mJ. The MOPFA uses a ~ 50 mW 1550 nm seed laser diode. The light pulses emitted by this laser are fed into erbium-doped fiber amplifier, with one or more stages, pumped by ~ 100 mW 980 nm laser diodes. To maintain a low average power, the minimum interval of time between pulses is increased compared to similar system.

The SDPM generates electrical pulses to encode the data according to a Pulse Position Modulation (PPM) scheme. The pulses are sent to the seed laser and can be generated with an accuracy better than 50 ps. The modulator is entirely implemented in a Field Programmable Gate Array (FPGA) to keep power, volume and complexity under control and allow flexible prototyping. The delays in the modulator are calibrated using a Delay Locked Loop (DLL). A compact, low power cesium oscillator, the Chip-scale Atomic Clock (CSAC)³, is used as reference for the DLL and for internal counting. Delays are combined in pair to increase the system resolution.

The MOCT is designed to be integrated with a CubeSat of at least 3U or on larger deep space spacecraft that are power-constrained. The selected wavelength and pulse energy levels make it compatible with existing ground terminals, for example those used for the LADEE mission^{4,5}.

SOFTWARE DEFINED PULSE MODULATOR

Modulation Scheme

The modulation scheme use the time interval between pulses to encode up to M different symbol, by placing a pulse in one of M time slots.¹ The unused time slot after the pulse can be skipped, the scheme is then called M-DPPM for M -slots Differential Pulse Position Modulation. Otherwise, if the slots after the pulse are still present, the scheme is called M-PPM for M -slots Pulse Position Modulation. As the time interval between pulses increases, so does the requirement for the frequency stability of the on-board clock. For intervals longer than 1 ms, the required Allan deviation is 10^{-8} , which is lower than typical quartz oscillators. We selected a cesium frequency source, the Chip Scale Atomic Clock (CSAC)⁴.

Architecture

Several treatments are required to generate electrical pulses from the raw input data. First, a forward error-correction code is applied to the data. Next, the M-PPM scheme is applied, at the digital level, transforming the data in a string of timestamps. In order to be converted in timed electrical pulses, the timestamps are then separated in two part. The first part is a counter value, this value is compared to a running counter. When it match, a base pulse is emitted. That base pulse then

travel through a variable delay chain. The second part of the timestamp is applied to the delay chain, to shifts the base pulse in time. Thanks to the delay chain, the pulse can be placed with a resolution higher than the period of one counter bit, and higher than what is allowed by the maximum system frequency.

The delay chain is specific to the device used for the modulator implementation and its layout must be done carefully. The modulator is implemented in a Microsemi SmartFusion 2.

Delay Chain

The current delay chain design. It is built around two device specific structures: The clock distribution network and the carry chain. Both run in parallel of the FPGA logic cells, in the same direction. Both are faster than the normal routing matrix. The row clock distribution lanes are slightly faster than the carry chain network, so a delay variation can be achieved by selecting in witch cell the signal cross from the clock distribution lane to the carry chain¹. The delay variation is plotted in figure 1. The delay chain have an overall delay of 12 ns for a variation of 6 ns. The output jitter is 3.5 ps, at the same level as the floor FPGA fabric jitter. The size of a 1-bit increment is 12 ps in average, however non-linearities of more than 90 ps are present, and, and the delay increase are monotonous.

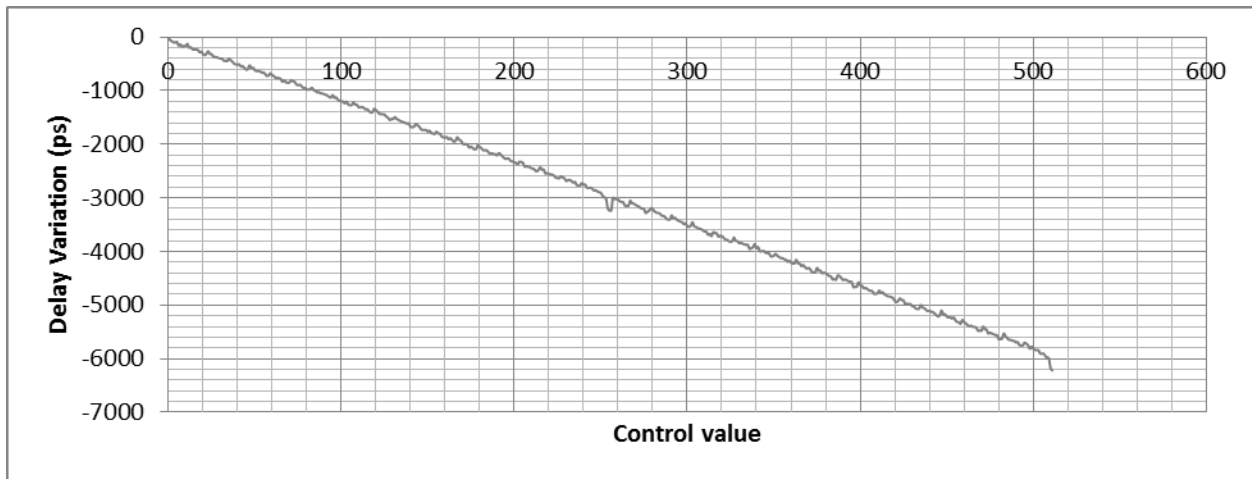


Figure 1: Delay chain propagation delay as a function of control input

Delay Locked Loop (DLL)

In any integrated circuit, the internal propagation delays are influenced by several factors. Aging and radiation damage, temperature, supply voltage and part-to-part variation are the dominating factors in silicon devices. In space applications, those factors are difficult to

control and their effect must be tracked to maintain accurate timing in orbit. Both cell-to-cell variation effects and global effects like temperature must be controlled. A circuit capable of measuring each delay element to obtain a calibration table and also capable to track environmental effects while modulating is

required. A Delay Locked Loop (DLL) circuit have been developed to measure and tracks delays.¹

In the DLL shown in Figure 2, a clock signal is generated by a variable frequency source. The variable frequency source is obtained by dynamically reprogramming a pair of Phase Locked Loops (PLLs). The PLLs use voltage controlled oscillator and frequency dividers to generate frequencies that are exact fractional multiples of a reference frequency. The PLLs are hardware, built-in module of the selected FPGA.

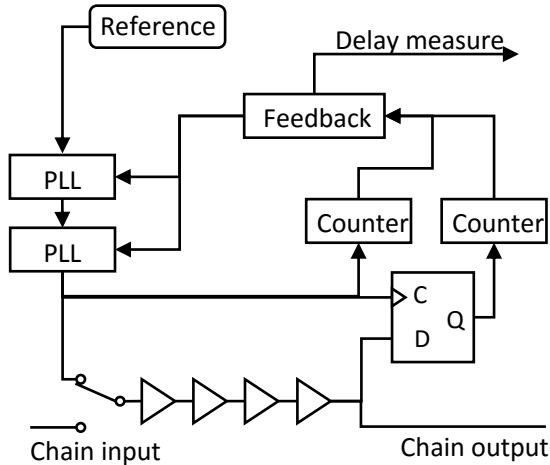


Figure 2: Delay Locked Loop block diagram¹

The variable clock signal is sent through the circuit under test, in our case the delay chain. The delayed clock signal is then compared to the original with an arbiter circuits, implemented here with a clocked latch. The latch can detect if a signal arrive before the other. By using a feedback to the variable frequency generator, it is possible to maintain equilibrium between the two paths, as seen in figure 3.

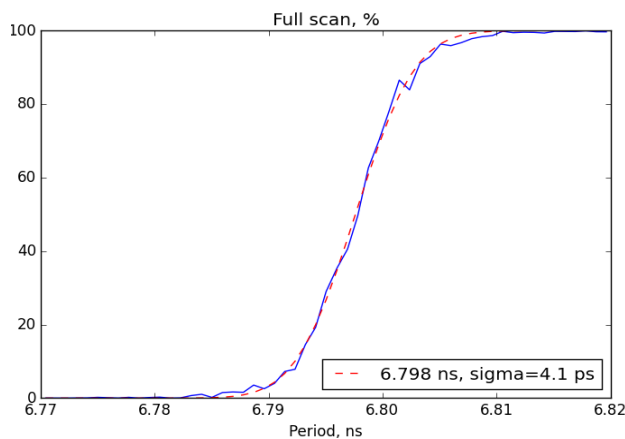


Figure 3: Fraction of ones at the DLL arbiter, close to the transition¹

In this state, the phase difference between the two paths is equal one clock period, or a multiple of that period. Figure 7 shows that the transition can be modeled as a cumulative Gaussian distribution. This distribution can be attributed to cycle-to-cycle jitter in the FPGA fabric, and latch meta-stability¹.

Combinatorial delay generation

Since two delay chains are used to obtain a delay range of 6 ns that can cover a complete counter period, it is possible to use advantageous combinations of settings to get closer to desired delay value. As shown in figure 4, the objective is to find a pair of settings that together give a target delay variation. This search is done for a large range of evenly spaced target delays to get a better scale of delays.

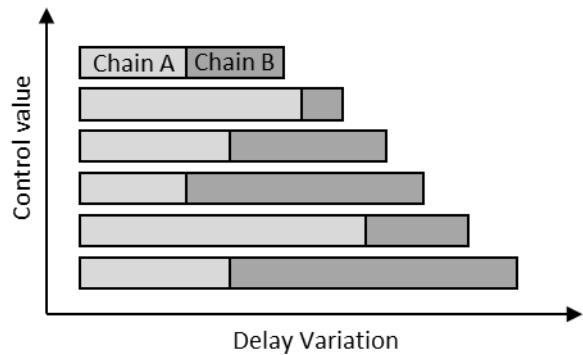


Figure 4: Examples of delay combinations

This is required since the residuals of the raw scale are large, with an integral nonlinearity of more than 90 ps. Chain designs with lower nonlinearity have large static (non-adjustable) delays that result in very low repetition rate and poor jitter performance.

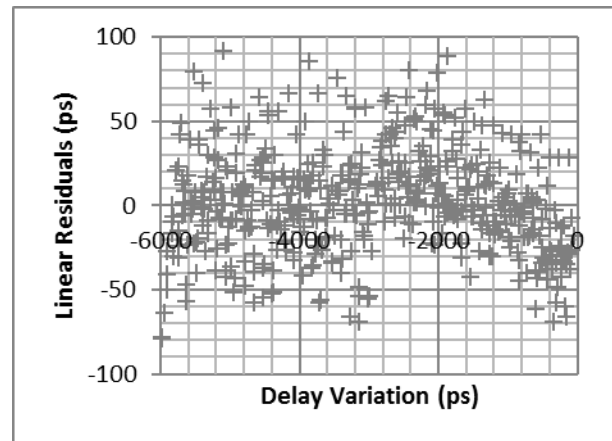


Figure 5: Linear residuals of raw delays

In theory, based on the internal measurements made using the delay locked-loop circuit, it is possible to reach extremely low deterministic jitter. Figure 6 shows the deterministic error of combinations of delays, assuming perfect measurements of the *raw* delays by the DDL circuit. A random jitter of up to 7 ps is also present.

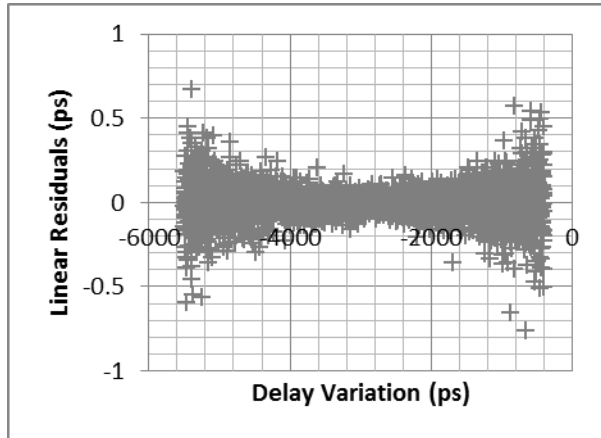


Figure 6: Linear residuals of theoretical combinations of delays

However, if the standard deviation of the DLL circuit measurements is below the picosecond-level, the bias of those measurements is usually larger than a picosecond. Figure 7 shows the deterministic error of combinations of delays, assuming perfect measurements of the *pairs* of delays by the DDL circuit.

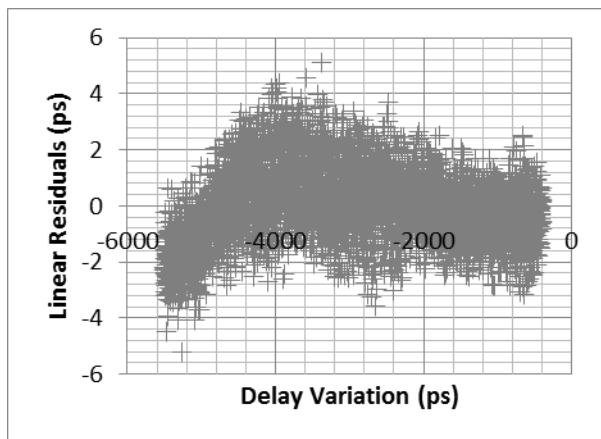


Figure 7: Linear residuals of measured combinations of delays

The comparison of expected and measured results for pairs of delays provides an estimate of the bias of the Delay Locked Loop circuit. Here, this bias is always less than 6 ps, with a standard deviation below 2 ps.

Even if the delay scale is not as good as depicted by Figure 6, the improvement over raw delays is still substantial. The raw delay and pair of delays scales are compared in table 1.

Table 1: Delay scale improvement

Value	Raw Delay	Delay Combination
LSB value	11.56 ps	1 ps (adjustable)
Number of entry	512	5100
Largest gap	> 70 ps	6.70 ps
Integral Non Linearity	96.7 ps	5.52 ps
STD of error	39.2 ps	1.35 ps

The DLL circuit can work at frequencies multiple of a base locking frequency, which can be assimilated to harmonics^[1]. Sampling several modes allow to estimate the bias of the measure at deferent frequency. A fixed known ballast delay could also be inserted to estimate the measurement bias with a different base and harmonics frequency

LASER SYTEM

Optical Power Requirements

MOCT provides pulsed optical communication for distant, power constrained small satellites. Four spacecraft-to-ground receiver distances to demonstrate the range of performance capabilities of the MOCT are (a) the maximum and (b) the minimum distances between Mars and the Earth (10 mJ and 0.2 mJ respectively), (c) the distance between the Moon and the Earth (10^{-5} mJ), and (d) a 450 km low Earth orbit altitude (10^{-14} mJ).¹ A MOPFA has been selected as the laser system for MOCT, over Q-switched lasers, since fiber amplifiers can accommodate arbitrary modulation and control pulse energy.

Master Oscillator Power Fiber Amplifier

In Figure 8, the continuous wave 980 nm pump laser stores energy in the Erbium doped fiber by 980 nm photons interacting with the electrons in the Erbium atoms and raising the electron's energy level. When the 1550 nm seed pulse enters the Erbium doped fiber, the 1550 nm photons interact with the elevated energy level electrons, and cause those electrons to drop their original energy level, releasing a photon at 1550 nm to join the seed pulse. The end product is a 1550 nm amplified pulse that is similar in shape to the seed pulse. The MOPFA allows for low average electrical power consumption to create high peak power optical pulses.

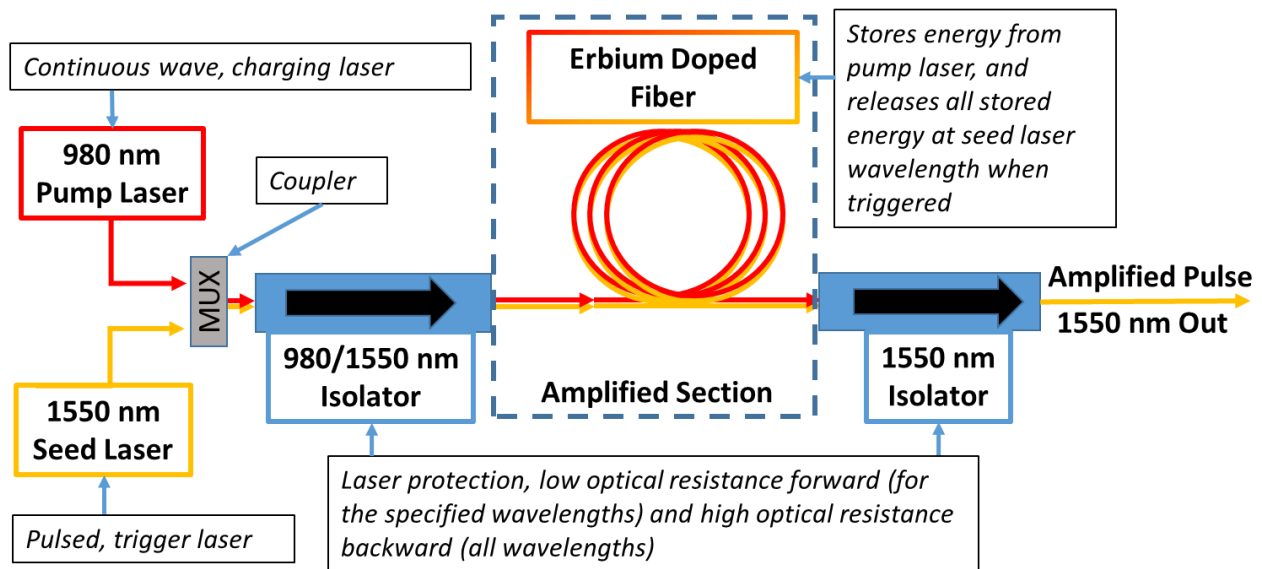


Figure 8 forward pumped, Master Oscillator Power Fiber Amplifier (MOPFA).

The pulse driver and seed laser convert the modulated data output data from the SDPM into optical pulses for the MOPFA. Currently, MOCT is utilizing ~50 mW seed laser driven by a Highland Technologies T165 pulse driver that can produce 200 ps pulses at a repetition rate of 250 MHz. The pump laser is responsible for controlling the amount of energy per pulse. The guard time, T_g , is how long the pump laser, at a particular power, needs to charge the fiber in order to achieve the desired pulse energy for the optical link.

When the fiber is saturated by the pump laser, then the maximum pulse energy is achieved. There is a tradeoff between T_g and power consumption, so MOCT will have the pump laser on marginally longer than T_g to meet the <10 W power consumption goal. After the isolator on the MOPFA, there will be ~8 cm telescope to expand and collimate the beam, in addition to keeping MOCT in the target volume of 2 liters.

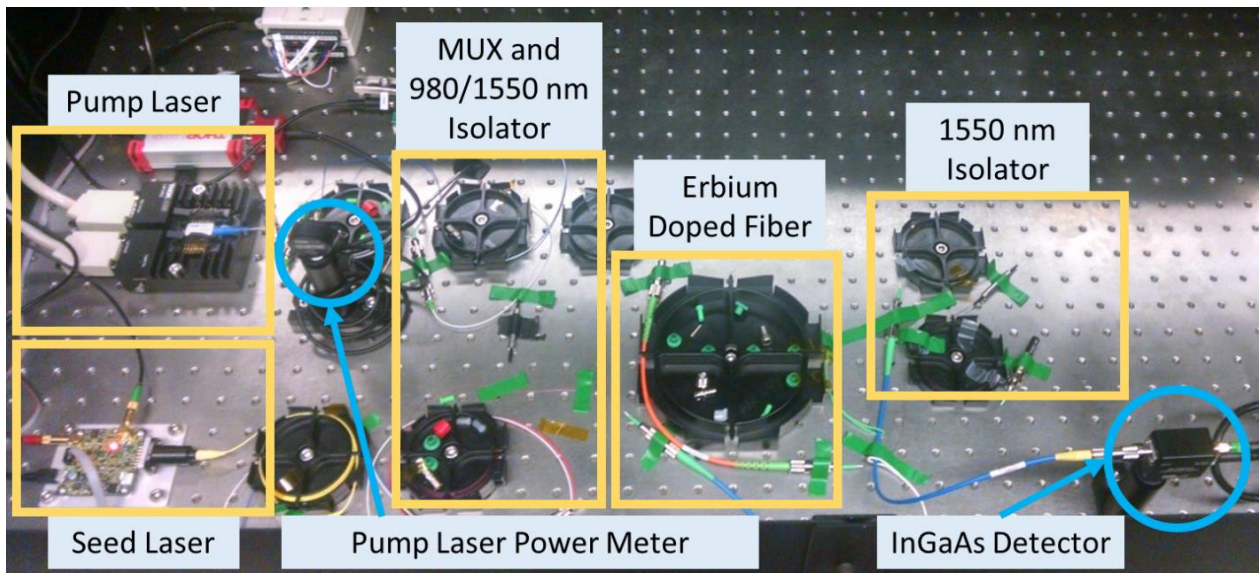


Figure 9 MOCT Benchtop MOPFA

Figure 9 is the MOCT Benchtop MOPFA at the University of Florida. This experiment has been

constructed in order to explore ways to maximize the M-number of MOCT by maximizing the peak power to

average power ratio. It contains the base components of MOPFA in Figure 8 with the addition of the pump laser power meter, which is attached to a 1% pickoff on the main pump laser fiber, and the InGaAs detector to see the output of the amplifier. The seed laser is 1544 nm and the pump is 976 nm, where both fall within the wavelength band pass filter of their respective isolators. The InGaAs detector was calibrated using the 1544 nm seed laser in continuous wave mode and the measured responsivity was 49.5 V/W.

Losses Characterization

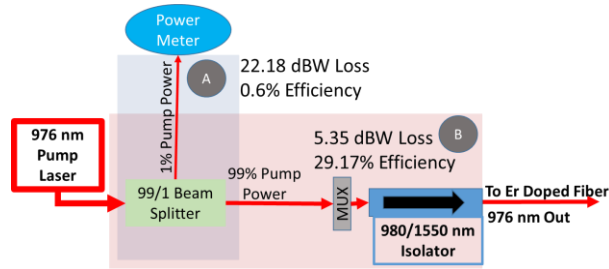


Figure 10 pump laser measurement setup

Figure 10 shows the power losses from the pump laser to the Erbium doped fiber. Region A represents the net loss from the output of the pump laser to the input of the power meter and Region B represents the net loss from the output of the pump laser to the input of the Erbium doped fiber. By utilizing the power meter and the losses in each region, the optical power entering the Erbium fiber from the pump laser can be monitored.

LABORATORY RESULTS

Modulator Performance

A prototype of the Software-Defined Pulse Modulator is shown in Figure 11. The important modulator performance metrics are its power consumption, maximum pulse rate, and timing accuracy.

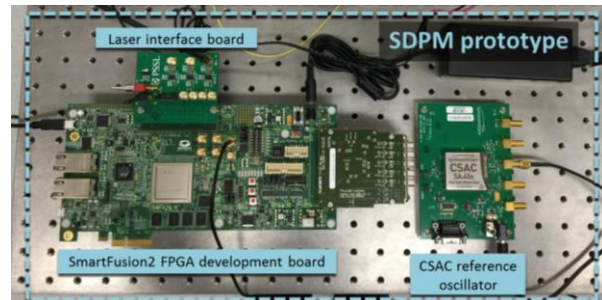


Figure 11: Software-Defined Pulse Modulator consisting of the SmartFusion2 FPGA, CSAC and laser driver interface board

The SDPM prototype is capable of producing sequences of electrical pulses with prescribed delays.¹ Figure 12 shows one such sequence with six pulses separated by 20 ns, 22 ns, 18 ns, 20 ns, and 18 ns respectively.

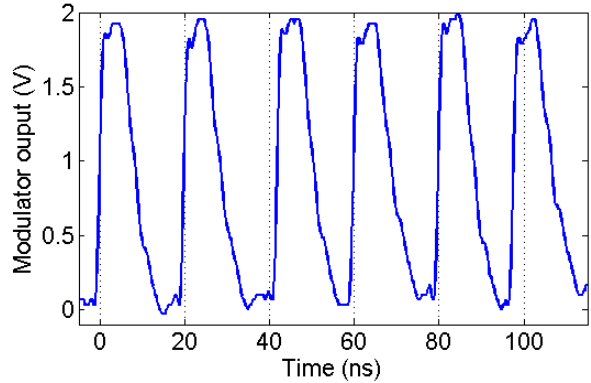


Figure 12: Variable delay pulse string¹

The maximum repetition rate is determined by the length of the delay chain. The current design uses a maximum delay of 12 ns. To ensure proper separation of pulses, the chain is run at a maximum of 50 million pulses per second. Several chains could run in parallel to further increase the maximum pulse rate. With the combinatorial delay generation approach, the objective is to get a total error, including both deterministic and random jitter, below 10 ps. The current measured jitter is 27 ps.¹

Maximum Peak Power Amplified Pulse

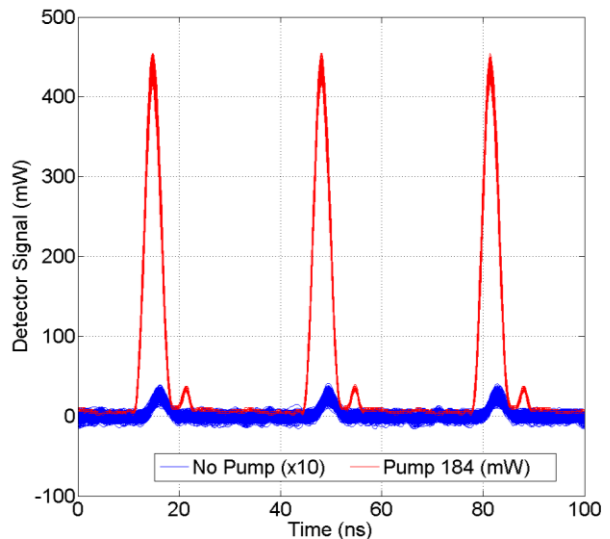


Figure 13 Maximum Pulse Power Amplification

The maximum pulse peak power measured was 435 mW (~21 dBW from the pump laser off pulse) on the

0.5 m fiber. This is a lower gain than many similar amplifiers, however by reducing reduce number of connections, matching refractive indices between components, and trying other Erbium fibers will likely increase amplification.

FUTURE WORK

The overall goal of this research is to elevate the technology readiness level of the MOCT to TRL 3 by the end of 2017. Over the next year we plan to integrate the modulator and its calibration circuit with a laser diode pulse driver in single system. That system will have volume and power requirements compatible with CubeSat. We will attempt to reduce the modulator jitter by improving the electrical interface between the FPGA and the pulse driver.

Also during this time, we plan to design and fabricate a prototype packaging for the MOCI that includes all of the components described in this paper plus an ~8 cm diameter beam expander. This packaging will be made consistent with a 2U CubeSat form factor so that it may be incorporated into a 3U or larger spacecraft platform.

Acknowledgments

The authors would like to thank Daniel Raible of the NASA Glenn Research Center for is technical expertise and support. This work is funded by NASA ECF Grant NNX14AO53G.

References

1. P. Serra, N. Barnwell, J.W. Conklin, "A novel, low power optical communication instrument for small satellites", Proceedings of the 29th Annual AIAA/USU Conference on Small Satellites, SSC15-VI-10, 2015.
2. J.W. Conklin, N. Barnwell, L. Caro, M. Carrascilla, O. Formoso, S. Nydam, P. Serra, N. Fitz-Coy, "Optical time transfer for future disaggregated small satellite navigation systems", Proceedings of the 28th Annual AIAA/USU Conference on Small Satellites, SSC14-IX-5, 2014.
3. Symmetricom, SA.45s CSAC, Chip Scale Atomic Clock Data Sheet, 2011.
4. Biswas A. and Kovalik, M.J., "The Lunar Laser OCTL Terminal (LLOT)," Proceedings of SPIE 8610, Free-Space Laser Communication and Atmospheric Propagation XXV, 86100O, 2013.
5. Li, J., Hylton, A., Budinger, J., Nappier, J., Downey, J., Raible, D., "Dual-Pulse Pulse Position Modulation (DPPM) for Deep-Space Optical Communications: Performance and

Practicality Analysis", NASA report NASA/TM—2012-216042, 2012.

6. Desurvire, E., "Analysis of Transient Gain Saturation and Recovery in Erbium-Doped Fiber Amplifiers," IEEE Photonics Technology Letters, 1(8), 1989.
7. Hemmati, H. editor, "Deep Space Optical Communications", Deep Space Communications and Navigation Series, NASA, 2005.